CHAPTER 198

SHORECIRC: A Quasi 3-D Nearshore Model

A.R. Van Dongeren[1], F.E. Sancho[2], I.A. Svendsen[3], and U. Putrevu[4]

ABSTRACT: A depth-integrated, short wave-averaged nearshore circulation model is presented, which includes the effects of the 3-D current structure over depth. The model includes the description of time-varying currents such as infra-gravity waves. Two numerical schemes are developed, which will be used for intercomparison in the absence of analytical solutions. An absorbing-generating boundary condition is developed based on the Method of Characteristics in order to allow propagating waves to leave the computational domain with a minimum of reflection while specifying incoming waves at the same boundaries. The model is tested for the time-varying start-up of a longshore current on a cylindrical coast, and the temporal development of both the cross-shore profiles of the longshore current and characteristic samples of the vertical structure of the velocity profiles are given.

INTRODUCTION

Shoaling, breaking, refraction and randomness of short waves are responsible for larger scale motions such as steady and unsteady currents and low frequency (infragravity) waves. These motions are all described by time-varying nearshore circulation models and can be observed as temporal and spatial variations of the short wave-averaged setup/setdown and longshore and cross-shore currents.

Two classes of models exist to describe these nearshore phenomena: *(i)* models that resolve the instantaneous state of motion, such as models based on the

[1]Graduate Student, Center for Applied Coastal Research, University of Delaware, Newark, DE 19716, USA. e-mail: apper@coastal.udel.edu

[2]Graduate Student, Center for Applied Coastal Research, University of Delaware, Newark, DE 19716, USA. e-mail: sancho@coastal.udel.edu

[3]Professor, Center for Applied Coastal Research, University of Delaware, Newark, DE 19716, USA. e-mail: ias@coastal.udel.edu

[4]Research Scientist, NorthWest Research Associates, Inc., Bldg. 7, Suite 220, 300 120th Avenue N.E., Bellevue WA 98009, USA. e-mail: putrevu@calvin.nwra.com

nonlinear shallow water equations or on the Boussinesq-equations and *(ii)* time-averaged models that calculate large scale motions due to short wave-induced forcing. The latter class can be further subdivided into two categories. Two-dimensional horizontal (2DH) models describe the depth-mean current and the surface elevation. They are based on the turbulence-averaged, depth-integrated, time-averaged Navier-Stokes equations. The second category, 2DV-models, have primarily been used to study the vertical structure of the cross-shore circulation (Svendsen (1984), Dally & Dean (1984), Stive & Wind (1986), Svendsen *et al.* (1987) and Svendsen & Hansen (1988)). Both types of models are an approximation of the fully 3D case, which until now has not been successfully modeled.

Quasi-3D models were developed to combine the effect of the vertical structure with the simplicity of 2DH models. In the approach by De Vriend & Stive (1987), the current is split into primary and secondary flow profiles based on the assumption that the primary velocity profiles are the same in the cross-shore and longshore direction. In a different approach, Svendsen & Lorenz (1989) determined the vertically-varying longshore and cross-shore currents separately under the assumption of weak dependence. They found that the total vertical current profile has a spiral shape (Fig. 1). Svendsen & Putrevu (1990) formulated a steady-state 3D nearshore circulation model using analytical solutions for the 3D current profiles in combination with a numerical solution of the depth-integrated 2D horizontal equations for a long straight coast. Sánchez-Arcilla *et al.* (1990, 1992) presented a similar concept. They split the current velocity into a depth-invariant component and a component with a vertical variation with zero mean flow integrated over the central layer. Putrevu & Svendsen (1992) and Svendsen & Putrevu (1994a) recognized that the current-current and current-wave interactions neglected in previous investigations induce a non-linear dispersion mechanism, which significantly augments the lateral turbulent mixing and explains the apparent difference in magnitude between the vertical and horizontal mixing.

In the present form, SHORECIRC is the time-dependent extension of the model presented by Svendsen & Putrevu (1994a). This comprehensive model is able to describe a number of nearshore phenomena such as surf-beat, edge waves and longshore currents while allowing for alongshore variations in the hydrodynamical conditions. By including finite amplitudes, random wave forcing, and the effects of the 3D current structure, it extends the description of these phenomena beyond the usual analytical solutions. The topography part of the model is presently configured for a cylindrical coast only, but will later be extended to cover arbitrary bottom topography as well. In the present paper we focus on the form of the 2DH equations, the generating-absorbing boundary condition used, and we test the model performance for a time-varying case of the longshore current on a long, straight beach.

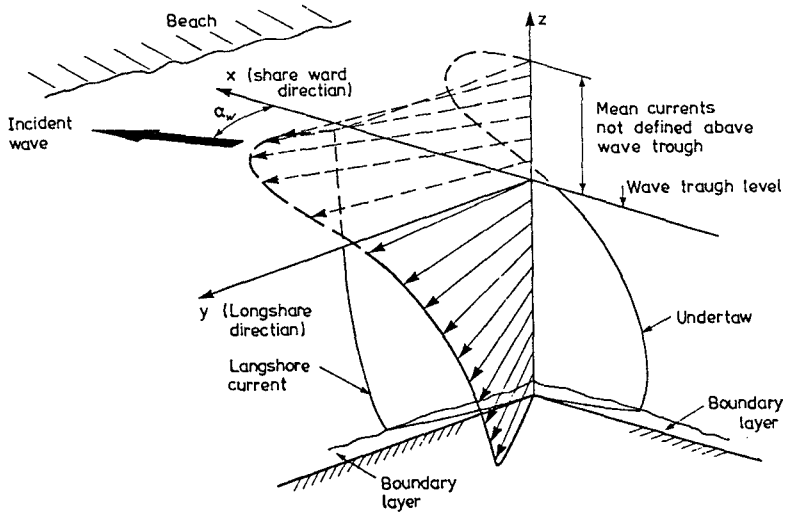

Figure 1: Three-dimensional structure of the current velocities in the surf zone (from Svendsen & Lorenz, 1989).

GOVERNING EQUATIONS

The depth-integrated, time-averaged mass and momentum equations read as follows:

$$\frac{\partial \bar{\zeta}}{\partial t} + \frac{\partial}{\partial x_\alpha}\left(\overline{\int_{-h_0}^{\zeta} V_\alpha \, dz} + Q_{w\alpha}\right) = 0 \tag{1}$$

$$\rho\frac{\partial \bar{Q}_\beta}{\partial t} + \rho\frac{\partial}{\partial x_\alpha}\overline{\int_{-h_0}^{\zeta} V_\alpha V_\beta \, dz} + \rho\frac{\partial}{\partial x_\alpha}\overline{\int_{\zeta_t}^{\zeta} u_{w\alpha}V_\beta + u_{w\beta}V_\alpha \, dz}$$
$$+ \rho g(\bar{\zeta} + h_0)\frac{\partial \bar{\zeta}}{\partial x_\beta} + \frac{\partial}{\partial x_\alpha}\left(S'_{\alpha\beta} - \overline{\int_{-h_0}^{\zeta} \tau_{\alpha\beta} \, dz}\right) - \tau_\beta^S + \tau_\beta^B = 0 \tag{2}$$

where the radiation stress $S'_{\alpha\beta}$ is given by

$$S'_{\alpha\beta} = \overline{\int_{-h_0}^{\zeta} (\rho u_{w\alpha}u_{w\beta} + \delta_{\alpha\beta}p) \, dz} - \delta_{\alpha\beta}\frac{1}{2}\rho g h^2 \tag{3}$$

which is equivalent to the definition used by Mei (1983).

In the above, V_α and $\bar{\zeta}$ represent the horizontal current velocity and the mean surface elevation, respectively, which is equivalent to the particle velocity

and wave surface elevation if an IG wave is considered. u_w is the short wave velocity, Q_α represents the total volume flux and Q_w is the volume flux due to the short wave motion. ζ_t is the elevation of the wave trough, $\tau_{\alpha\beta}$ is the Reynolds stress, h_o is the still water depth, while τ_β^S and τ_β^B represent the surface (e.g. wind) and the bottom shear stresses, respectively. The overbar denotes short wave averaging and the subscripts α and β denote the directions in a horizontal Cartesian coordinate system. See Figure 2 for a definition sketch.

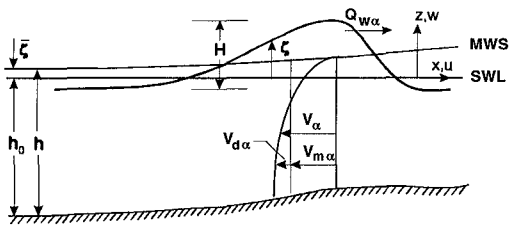

Figure 2: Definition sketch.

The form (2) of the momentum equation is written in terms of V_α which is the current defined in the traditional way: the net velocity at any point below wave trough level over and above the purely oscillatory wave motion (i.e. $\bar{u}_w = 0$). For the general case of depth varying currents it is convenient to split this current into a depth uniform and depth varying component:

$$V_\alpha = V_{m\alpha}(x, y, t) + V_{d\alpha}(x, y, z, t) \tag{4}$$

where

$$V_{m\alpha} = \frac{\bar{Q}_\alpha - Q_{w\alpha}}{h} \tag{5}$$

and

$$Q_{w\alpha} = \overline{\int_{-h_0}^{\zeta} u_{w\alpha}\, dz} \tag{6}$$

It may be verified that

$$\int_{-h_0}^{\bar{\zeta}} V_\alpha\, dz = \bar{Q}_\alpha - Q_w \qquad \text{and} \qquad \int_{-h_0}^{\bar{\zeta}} V_{d\alpha}\, dz = 0 \tag{7}$$

Then (2) may be written as

$$\rho\frac{\partial\bar{Q}_\beta}{\partial t}+\rho\frac{\partial}{\partial x_\alpha}\left(\frac{\bar{Q}_\alpha\bar{Q}_\beta}{h}\right)+\rho\frac{\partial}{\partial x_\alpha}\int_{-h_0}^{\bar{\zeta}}V_{d\alpha}V_{d\beta}\,dz$$
$$+\rho\frac{\partial}{\partial x_\alpha}\overline{\int_{\zeta_t}^{\zeta}u_{w\alpha}V_{d\beta}+u_{w\beta}V_{d\alpha}\,dz}+\rho g\left(\bar{\zeta}+h_0\right)\frac{\partial\bar{\zeta}}{\partial x_\beta}$$
$$+\frac{\partial}{\partial x_\alpha}\left(S_{\alpha\beta}-\overline{\int_{-h_0}^{\zeta}\tau_{\alpha\beta}\,dz}\right)-\tau_\beta^S+\tau_\beta^B=0 \tag{8}$$

where $S_{\alpha\beta}$ is the radiation stress defined by

$$S_{\alpha\beta}=S'_{\alpha\beta}-\rho\frac{Q_{w\alpha}Q_{w\beta}}{h} \tag{9}$$

which is the definition used by Phillips (1977).

The integrals in (8) represent the effects of the depth-varying currents. The rest of the terms are essentially equivalent to the terms found by Phillips (1977) and Mei (1983).

The equations (1) and (8) are solved by finite differences for the time and space variation of $\bar{\zeta}$ and $\bar{Q}_\alpha$ in combination with an analytical solution for the current distribution along the vertical, which is given in terms of eigenfunction expansions. This analytical solution includes integration constants that are in turn determined from the numerical solution of the depth-integrated equation (8). The details of this are left out for reasons of space limitation (Svendsen & Putrevu, 1994b and Putrevu & Svendsen, 1994).

NUMERICAL SCHEMES

Two numerical schemes have been developed: a second order, explicit predictor-corrector method and a second order, ADI staggered-grid scheme. This allows us to compare the two numerical solutions to each other when an analytical solution for the 2DH current pattern is not readily obtained, for instance in cases of random wave forcing or a complicated bathymetry. Both schemes have inherent advantages and drawbacks. While simpler, the explicit method has a Courant-Friedrichs-Lewy (CFL) limitation on its stability, which sets an upper limit on the time-step allowed. Typically we use a Courant number of 0.35 - 0.7. The ADI method, which has no CFL limit, is both more robust and more complicated for the nonlinear terms. Hence it can be operated at even larger Courant numbers, although it loses accuracy if the Courant number is increased too much.

ABSORBING-GENERATING BOUNDARY CONDITION

In order to be able to model a limited coastal region in an otherwise large ocean, it is necessary to establish boundary conditions along the open ocean-side boundaries that satisfy two criteria:

1. The region outside the computational domain only influences the motion inside through incident (long) waves and currents, which we know and specify along the open boundaries.
2. (Long) waves propagating out of the computational region must be allowed to propagate freely through the open ocean-side boundaries with minimal reflection.

Thus this boundary condition must be able to generate a specified long wave and simultaneously absorb outgoing waves. Such a generating-absorbing boundary condition is derived below based on the Method of Characteristics (Abbott, 1979; Verboom *et al.*, 1981).

We first notice that the open boundaries are established so that near these boundaries the dominating terms in the continuity and momentum equations are the terms corresponding to the nonlinear shallow water (NSW) equations. Introducing $\bar{u}_\alpha = \frac{\bar{Q}_\alpha}{h}$, where h denotes total water depth, we can thus write (1) and (8) as

$$\frac{\partial \bar{\zeta}}{\partial t} + \frac{\partial\, h\, \bar{u}_\alpha}{\partial x_\alpha} = 0 \tag{10}$$

$$\frac{\partial \bar{u}_\beta}{\partial t} + \bar{u}_\alpha \frac{\partial \bar{u}_\beta}{\partial x_\alpha} = -g \frac{\partial \bar{\zeta}}{\partial x_\beta} + f_\beta \tag{11}$$

where f_β represents forcing terms for the motion which include the radiation stress terms, the $V_{d\alpha}$-integrals, the bottom and wind shear stresses and the bottom slope term, all included in the original equations.

In characteristic form these equations can be written as:

$$\frac{\partial \beta^+}{\partial t} = -(\bar{u} + c)\frac{\partial \beta^+}{\partial x} - \bar{v}\frac{\partial \beta^+}{\partial y} - c\frac{\partial \bar{v}}{\partial y} + g\frac{\partial h_o}{\partial x} + F_{\beta^+} \tag{12}$$

$$\frac{\partial \beta^-}{\partial t} = -(\bar{u} - c)\frac{\partial \beta^-}{\partial x} - \bar{v}\frac{\partial \beta^-}{\partial y} + c\frac{\partial \bar{v}}{\partial y} + g\frac{\partial h_o}{\partial x} + F_{\beta^-} \tag{13}$$

$$\frac{\partial \gamma}{\partial t} = -\bar{u}\frac{\partial \gamma}{\partial x} - \bar{v}\frac{\partial \gamma}{\partial y} - g\frac{\partial \bar{\zeta}}{\partial y} + F_\gamma \tag{14}$$

where β^+ in (12) is the ingoing Riemann-invariant $\bar{u} + 2c$ and $c = \sqrt{g(h_0 + \bar{\zeta})}$. $\beta^- = \bar{u} - 2c$ and $\gamma = \bar{v}$ are the Riemann-invariants of (13) and (14). The forcing terms $F_{\beta+}$, $F_{\beta-}$ and F_γ originate from the f-terms in (11). Because of these terms, the invariants should actually be called *variables*. It turns out that the γ-equation is the y-momentum equation itself. See Figure 3 for a definition sketch showing the characteristics. Note that the Riemann-variants β^+ and β^- are not related to the subscript β used in (1) through (11).

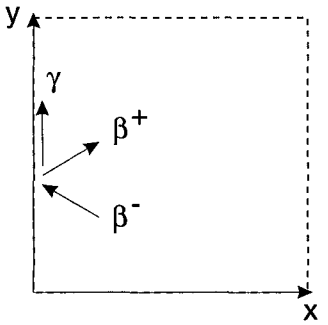

Figure 3: Definition sketch of the characteristics.

From the Riemann variable β^-, which propagates along a trajectory in the negative x-direction and is updated by (13), we can derive a relationship between the flux of the outgoing wave (subscripted 'r' in the following) and the incoming wave (subscripted 'i'). Assuming linear superposition of these waves

$$\vec{Q} = \vec{Q}_i + \vec{Q}_r \tag{15}$$

and substituting the identities

$$\vec{Q}_i = \vec{c}\zeta_i \qquad \vec{Q}_r = -\vec{c}\zeta_r \tag{16}$$

which are valid irrespective of wave theory and only assume constant form, we get

$$|Q_r|\,(\cos\theta_r + 1) = h_o\beta^- - |Q_i|(\cos\theta_i - 1) + 2h_o\sqrt{gh_o} + O\left(\frac{\bar{\zeta}}{h_o}\right)^2 \tag{17}$$

where θ_i and θ_r are defined as the angles between the normal to the boundary and

the incoming and outgoing waves, respectively. From the y-momentum equation (14) we then get

$$|Q_r| \sin\theta_r = Q_y - Q_{iy} \tag{18}$$

where $Q_y = \bar{v}(h_o + \zeta)$. From (17) and (18) we can find the unknowns $|Q_r|$ and θ_r iteratively. With the incoming wave known through specification, and integrating (13) and (14) in time, the boundary values of total fluxes Q_x and Q_y, and the surface elevation $\bar{\zeta}$, are determined at the next time step. This boundary condition is essentially a generalized version of the condition derived for the 1-D case by Kobayashi *et al.* (1987).

Two cases have been run to test this absorbing-generating boundary condition. In the first case, linear waves were generated under various angles at the $x = 0$ and $y = 0$ boundaries. They were propagated over a flat bottom using the linearized equations and absorbed at the $x = L_x$ and $y = L_y$ boundaries. This tests the absorbing capability of the boundary condition. The parameters used were: wavelength $\lambda = 50\,m$, domain lengths $L_x = L_y = 2\,\lambda$, $h_o = 1\,m$, $T = \lambda / \sqrt{g\,h_o}$, $A = 0.01\,m$, $\Delta x = \Delta y = \frac{\lambda}{30}$ and $C_r = 0.6$. Figs. 4 a-c show the instantaneous water surface for three selected angles $\theta = 0^o, 30^o$ and 75°, where θ is defined as the angle between the incident wave ray and the y-axis. Reflections from the boundaries are barely visible.

To calculate the reflection coefficient, a time series was taken at a point on the boundary. Then the domain was extended to be effectively infinite and another time series was taken at the same point. Following Verboom & Slob (1984), the reflection coefficient is then defined as the maximum of the difference of the two time series normalized by the amplitude of the original wave:

$$R = \frac{max\ \Delta\zeta(t)}{A} \tag{19}$$

Fig. 4 d shows this reflection coefficient R (indicated by the dots) as a function of the angle of incidence θ.

A comparison is made to the widely-used Sommerfeld radiation condition

$$\left(\frac{\partial}{\partial t} + \frac{c}{\cos\theta_r}\frac{\partial}{\partial x}\right)^n u = 0 \tag{20}$$

where n indicates the order of the approximation of the boundary condition. For instance, the radiation condition that was introduced by Engquist & Majda (1977) has $n = 2$. The theoretical reflection coefficient of this type of condition, which can be calculated as (Higdon, 1986)

$$R = \left|\left(\frac{\cos\theta_r - 1}{\cos\theta_r + 1}\right)^n\right| \tag{21}$$

is shown in Fig. 4 d for three values of n, indicated by the solid lines. The figure shows that the present condition based on the Method of Characteristics has much better absorption capabilities than the Sommerfeld condition. The latter gives large reflection coefficients for large angles and is fully reflecting for waves propagating parallel to the boundary. Note that the reflection, as calculated by (19), includes truncation and other numerical errors, while R, as calculated by (21), is theoretical only. This probably causes the better performance of the Sommerfeld condition at small angles.

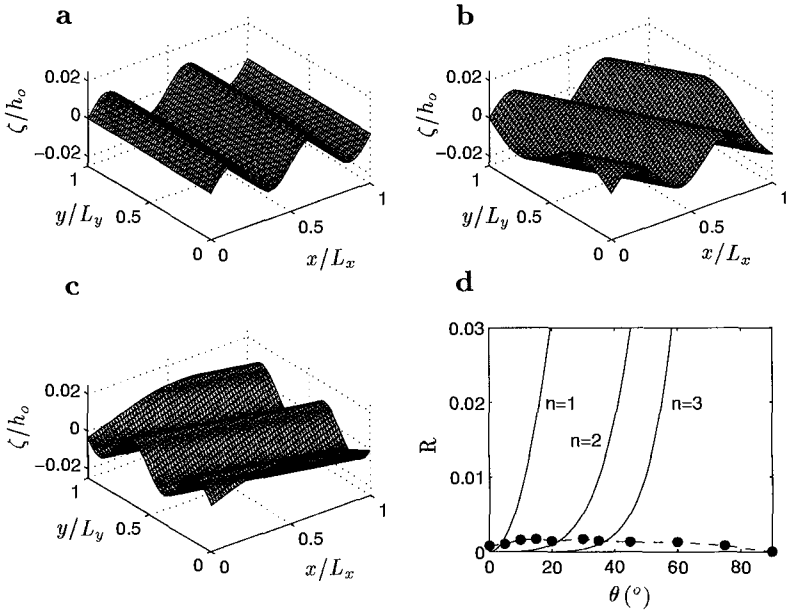

Figure 4: (a) Instantaneous water surface for $\theta = 0^o$. (b) Same for $\theta = 30^o$. (c) Same for $\theta = 75^o$. (d) Reflection coefficients versus angle θ, —: Eq. (21), •: present model.

In a second test, waves are simultaneously generated and absorbed at the $x = 0$ boundary. From a cold start, waves are generated under an angle of 0° from $t = 0\,T - 19\,T$ and are reflected off a wall at $x = L_x$. Parameters used are: wavelength $\lambda = 50\,m$, domain lengths $L_x = 3.3\,\lambda$ and $L_y = 0.2\,\lambda$, $h_o = 1\,m$, $T = \lambda\,/\,\sqrt{g\,h_o}$, $A = 0.01\,m$, $\Delta x = \Delta y = \frac{\lambda}{60}$ and $C_r = 0.6$. Fig. 5 a shows the wave propagating in $+x$-direction at $t = 2\,T$ and Fig. 5 b the resulting standing wave. At $t = 19\,T$ the incoming wave was turned off instantaneously (causing a minor disturbance wave that is visible in Fig. 5 c where a wave propagating in the negative x-direction is trailed by higher frequency disturbances). The central

part of the time series (taken at $x = 0$, $y = \frac{L_y}{2}$) in Fig. 5 d shows the standing wave whose amplitude is equal to the analytical solution within a few percent. It also shows that the transients radiate out with very little reflection. Still-water conditions are reached fairly quickly after the generated waves leave the domain.

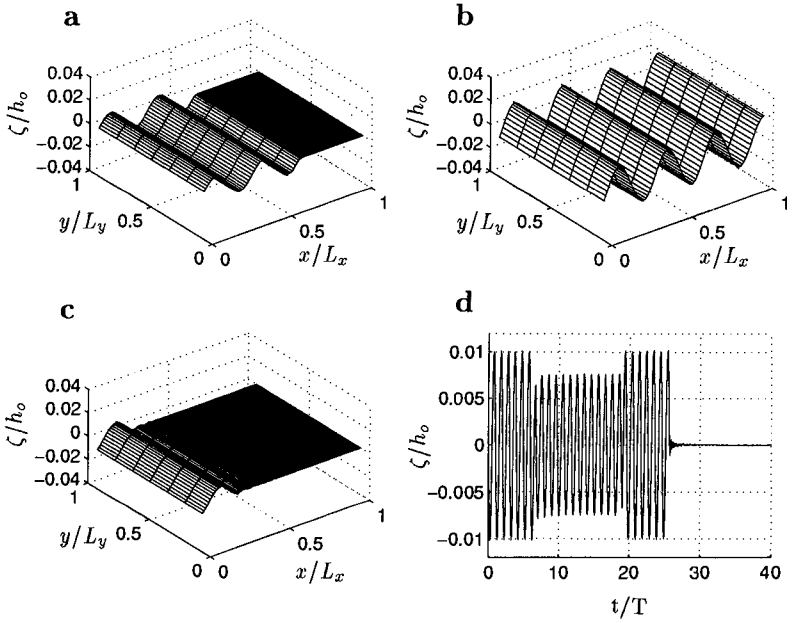

Figure 5: (a) Instantaneous water surface at $t = 2T$. (b) Same for $t = 19T$. (c) Same for $t = 25T$. (d) Time series at ($x = 0$, $y = \frac{L_y}{2}$).

These tests show that the numerical boundaries can be placed close to the regions of interest, which limits the computational time for the model.

TEST CASE: LONGSHORE CURRENTS

As a formal test of the time-dependent equations (1) and (8), we studied the start-up of a longshore current on a cylindrical coast induced by imposing short wave forcing in a region at rest at $t = 0$. The parameters and assumptions used are the same as those in Chapter 4 of Svendsen & Putrevu (1994a), called SP94 in the following, except that here the depth-invariant longshore velocity V_0 (see their (2.6)) is explicitly defined as the depth mean longshore velocity.

Fig. 6 a shows the surface elevation versus normalized time for a number of

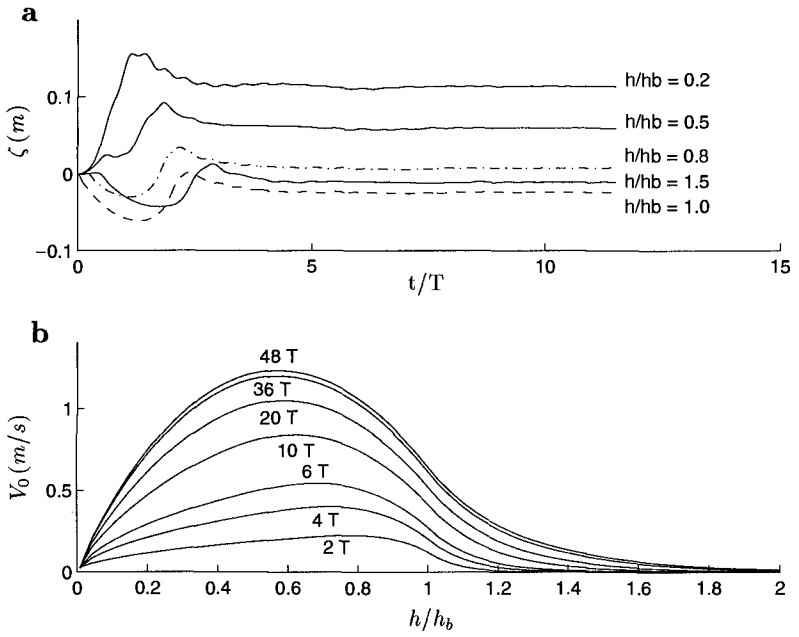

Figure 6: (*a*) Surface elevation versus time for cross-shore positions indicated in the figure. (*b*) Cross-shore variations of the longshore current velocities for different time-steps as indicated in the figure.

points in the domain. The normalizing time-scale T is defined as the ratio of the surf-zone width to the long wave celerity at the breakpoint. It is also seen that the impulsive application of the short wave forcing at $t = 0$ initiates a surge in the mean surface elevation. After reflection from the beach, it propagates seawards and is absorbed by the ocean-side boundary condition. The steady-state in the set-up is reached in about $7\,T$. The longshore current evolution in Fig. 6 b, however, does not attain steady-state until about $50\,T$, which indicates a difference in time-scales of cross-shore and longshore motion. In fact, the steady-state is only approached asymptotically as the net forcing of bottom friction and the radiation stress decreases to zero. The figure clearly shows that the turbulent and dispersive mixing, ν_{tx} and D_c (defined in SP94 Eq. (2.22)), cause a spreading of momentum (i.e. longshore current velocity) away from the breakpoint but the momentum spreads relatively slowly, in particular outside the surf-zone.

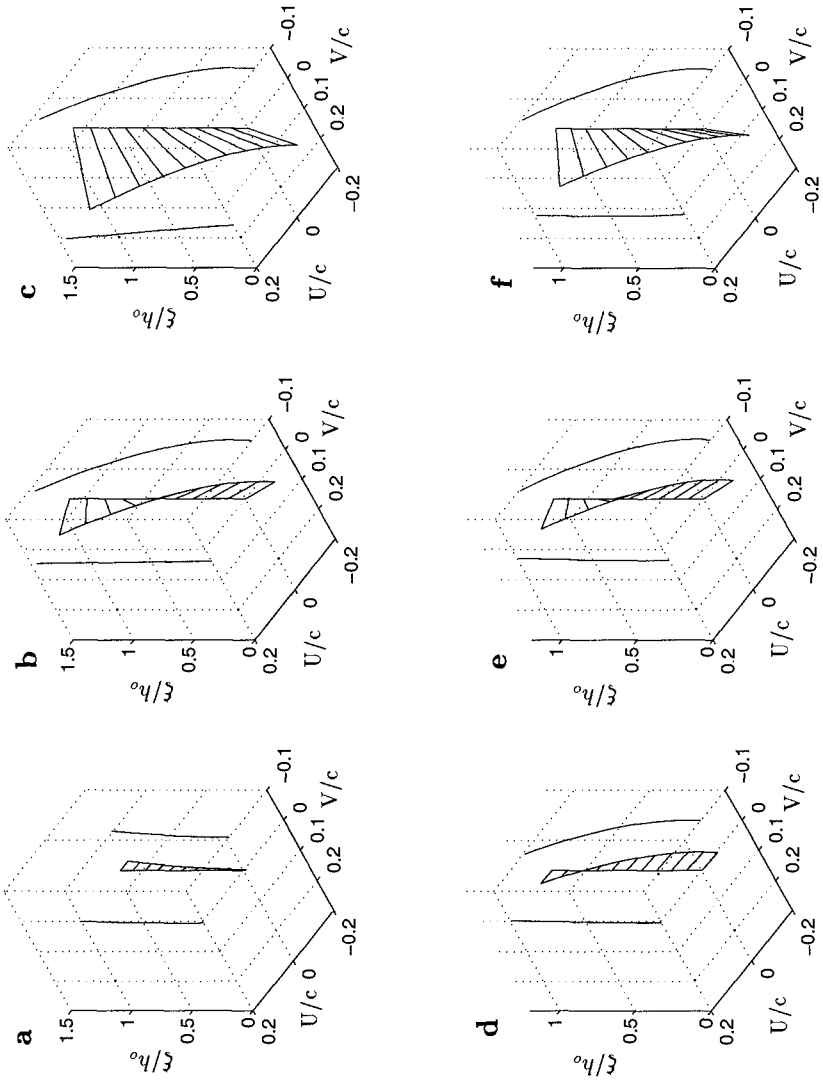

Figure 7: (*a*) Three-dimensional current spiral for $\frac{h_o}{h_b} = 0.24$ at $t = 0.2T$. (*b*) Same for $t = 4T$. (*c*) Same for $t = 48T$.(*d*) Three-dimensional current spiral for $\frac{h_o}{h_b} = 0.98$ at $t = 0.2T$. (*e*) Same for $t = 4T$. (*f*) Same for $t = 48T$.

The slow development in the flow implies that the vertical velocity profiles can be considered a quasi-steady response to the instantaneous forcing, including the gradients of the mean water surface. Thus, using SP94's expressions for the undertow and longshore velocity with time-varying coefficients, we can calculate the change in the 3-D current profiles as time progresses. Figs. 7 a-c show three snapshots of the 3-D current spiral for a position close to shore. Figs. 7 d-f show the spirals at the same times for a position in the surf-zone near the breakpoint. The cross-shore and longshore current profiles are also shown as projections. The current velocities, U and V, are normalized by the local wave celerity and ξ, the vertical position above the bed, is normalized by the still water level h_o. Figs. 7 a and 7 d for $t = 0.2T$ show that initially the flow is almost entirely in the cross-shore direction. At $t = 4T$, the steady-state in the set-up, and consequently in the undertow profile, is not yet reached and the magnitude of the longshore current is increasing rapidly (Figs. 7 b and 7 e). At $t = 48T$, both the undertow and the longshore current have reached steady-state (Figs. 7 c and 7 f). Notice that the longshore current profile in Fig. 7 c is pitched forward, whereas the one in Fig. 7 f is tilted back slightly. This is important since the sign of the vertical gradient of V indicates a sign switch in the dispersive effect, which is known to control the mixing (SP94). We see that the different time scales for the cross- and longshore motion cause the velocity to change quite significantly during the start-up of the longshore current. With time-varying forcing from random waves, the variation will probably be less dramatic. However, the results for the 2DH case with weak wave groups analysed by Svendsen and Putrevu (1994b) suggest that the vertical currents profiles can vary significantly.

For completeness it is mentioned that these computations were performed with a very short coast to ensure that no instabilities in the form of shear waves developed.

CONCLUSIONS

A time-dependent, short wave-averaged quasi-3D model is presented that governs nearshore circulation processes as well as infra-gravity waves. An absorbing-generating boundary condition has been developed that allows waves to leave the domain with very little reflection while simultaneously specifying an incoming wave. This makes it possible to choose the model boundaries close to the area of interest, thus limiting the computational effort required. The time-dependent model is tested for the start-up of a longshore current on a long straight coast. The vertical velocity profiles are shown to change significantly as the current evolves.

ACKNOWLEDGMENTS

This work is a result of research sponsored by NOAA Office of Sea Grant, De-

partment of Commerce, under Award. No. NA 16 RG 0162 (Project No. R/OE-15) and by the U.S. Army Research Office, University Research Initiative under Contract No. DAAL03-92-G-0016. F.E. Sancho held a scholarship from the Portuguese Research Council, and his contribution was carried out under the MAST G8 Coastal Morphodynamics Programme, funded by the Commission of European Communities, Directorate General for Science, Research and Development (contract no. MAS2-CT92-0027). U. Putrevu was funded by ONR Coastal Sciences (contract number N00014-94-C0004). The U.S. Government is authorized to produce and distribute reprints for government purposes notwithstanding any copyright notation that may appear herein.

REFERENCES

Abbott, M.B. (1979). Computational Hydraulics. Elements of the Theory of Free Surface Flow. Pitman Publishing, 324 p.

Anderson, D.A., J.C. Tannehill and R.H. Pletcher (1984). Computational fluid mechanics and heat transfer. Hemisphere Publishing Corp., New York, 599 p.

Dally, W.R. and R.G. Dean (1984). Suspended sediment transport and beach profile evaluation. *Journal of Waterway, Port, Coastal and Ocean Engineering, ASCE, 110*, pp. 15-33.

De Vriend, H.J. and M.J.F. Stive (1987). Quasi-3D modelling of nearshore currents. *Coastal Engineering, 11*, pp. 565-601.

Engquist, B. and A. Majda (1977). Absorbing boundary conditions for the numerical simulation of waves. *Math. Comp., vol. 31, no. 139*, pp. 629-651.

Higdon, R.L. (1986). Absorbing boundary conditions for difference approximations to the multi-dimensional wave equation. *Math. Comp., vol. 47, no. 176*, pp. 437-459.

Kobayashi, N., A.K. Otta and I. Roy (1987). Wave reflection and run-up on rough slopes. *Journal of Waterway, Port, Coastal and Ocean Engineering, ASCE, vol. 113, no. 3*, pp. 282-298.

Mei, C.C. (1983). The applied dynamics of ocean surface waves. John Wiley and Sons, New York, 740 pp.

Phillips, O.M. (1977). The dynamics of the upper ocean. Cambridge University Press, 336 pp.

Putrevu, U. and I.A. Svendsen (1992). A mixing mechanism in the nearshore region. *Proc. of the 23rd International Conference on Coastal Engineering*, pp. 2758-2771.

Putrevu, U. and I.A. Svendsen (1994). Infragravity velocity profiles in the surf-zone. *Submitted for publication.*